Variability and Controls on the Matrix Permeability of the Doig Formation in Northeastern British Columbia

P.L. Silva, The University of British Columbia, Vancouver, BC, pablols@alumni.ubc.ca

R.M. Bustin, The University of British Columbia, Vancouver, BC

Silva, P.L. and Bustin, R.M. (2019): Variability and controls on the matrix permeability of the Doig Formation in northeastern British Columbia; *in* Geoscience BC Summary of Activities 2018: Energy and Water, Geoscience BC, Report 2019-1, p. 21–28.

Introduction

The Lower to Middle Triassic Doig Formation of the Western Canada Sedimentary Basin (WCSB) extends continuously across northeastern British Columbia (BC) and west-central Alberta. Historically, the Doig and the underlying Montney formations were viewed as source rocks for other conventional reservoirs in the basin, mainly in other Triassic, and Cretaceous strata (Du Rouchet, 1985; Creaney and Allan, 1990; Riediger et al., 1990; Edwards et al., 1994). There has also been some limited hydrocarbon production from the conventional sandstone bodies in the Doig (Marshall et al., 1987; Walsh et al., 2006; Chopra et al., 2014). With the industry shifting the focus of development to unconventional reservoirs, the Doig Formation has been recognized as an important resource of gas and natural-gas liquids (NGL). The Gas Technology Institute (Faraj et al., 2002) estimated the Doig total gas-in-place at 4 trillion m^3 (140 tcf), while Walsh et al. (2006) estimated it as ranging from 1.1 to 5.7 trillion m^3 (40–200 tcf). A more recent study by the United States Energy Information Administration (2013) estimated 2.8 trillion m^3 (100 tcf) of gas-in-place for the Doig Phosphate Zone alone. The unconventional portion of the Doig is a relatively new play and thus, the distribution of its properties has not been extensively studied nor is it well understood. Basin-scale studies that focus on the entire Doig succession and the variation in its properties are notably absent in the literature. The present study aims to characterize the range and variability of the matrix permeability of the Doig Formation, as well as explain the geological factors that control this variability in terms of lithology, mineralogy, organic matter, porosity and pore-size distribution.

Geological Framework

The sedimentation in the Triassic of the WCSB is marked by a transition from carbonate-dominated intra-cratonic and passive-margin conditions, predominant during the Paleozoic, to a siliciclastic-dominated relatively active embryonic foreland basin. The general paleogeographic configuration of the Triassic in the WCSB was that of a westward-deepening continental shelf margin. This westward facing margin under the influence of trade winds, seasonal climatic aridity and coastal cold-water oceanic upwelling, was characterized by low fluvial input, dominantly fine-grained siliciclastic sedimentation in marine shelves and ramps, with extensive associated eolian and evaporitic environments (Marshall et al., 1987; Henderson, 1989; Davies, 1997).

The Middle Triassic Doig Formation is part of the Diaber Group along with the underlying Montney Formation (Figure 1). This group was defined by Armitage (1962), who redefined the original Toad–Grayling Formation equivalents in the subsurface as the Doig and Montney formations. The lower boundary of the Doig corresponds to the base of a phosphatic zone, which was later informally named Doig Phosphate Zone (DPZ) by Creaney and Allan (1990). The Triassic succession was deposited in a series of three major third- or fourth-order transgressive-regressive cycles (Gibson and Barclay, 1989; Edwards et al., 1994). The interval from the Doig through the Halfway and Charlie Lake formations corresponds to the second cycle and the DPZ represents a condensed section formed during the initial transgression of the second cycle (Gibson and Barclay, 1989).

The main structural elements that influenced the distribution of the WCSB Triassic interval were the underlying Devonian Leduc and Swan Hills reefs, and the Mesozoic reactivation of the Mississippian Dawson Creek graben complex (DCGC), which includes the Fort St. John graben (FSJG) and the Hines Creek graben. The DCGC formed in response to localized subsidence in the Peace River Embayment. The DCGC faults continued to be active during the Triassic, imposing significant controls on the distribution of sediments (Marshall et al., 1987; Barclay et al., 1990; Davies, 1997; Eaton et al., 1999). The Devonian reefs exerted a topographic influence on Triassic sedimentation by controlling facies change (Davies, 1997), and may also have influenced subsidence rates and, hence, thickness variation.

This publication is also available, free of charge, as colour digital files in Adobe Acrobat® PDF format from the Geoscience BC website: http://www.geosciencebc.com/s/SummaryofActivities.asp.

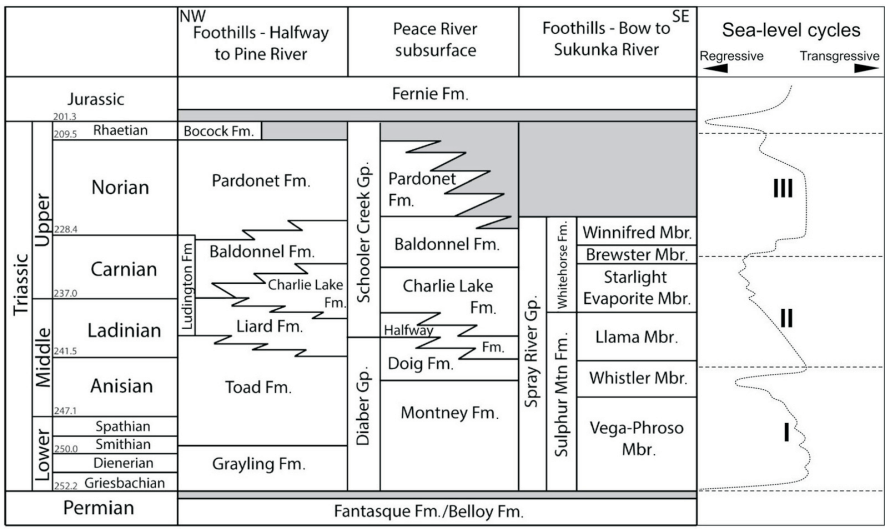

Figure 1. Stratigraphic chart of the Triassic, correlating the surface and subsurface relationships of British Columbia and the surface relationships of Alberta (after Gibson and Barclay, 1989; Golding et al., 2015). Eustatic level based on Hardenbol et al. (1998). Abbreviations: Fm., Formation; Gp., Group.

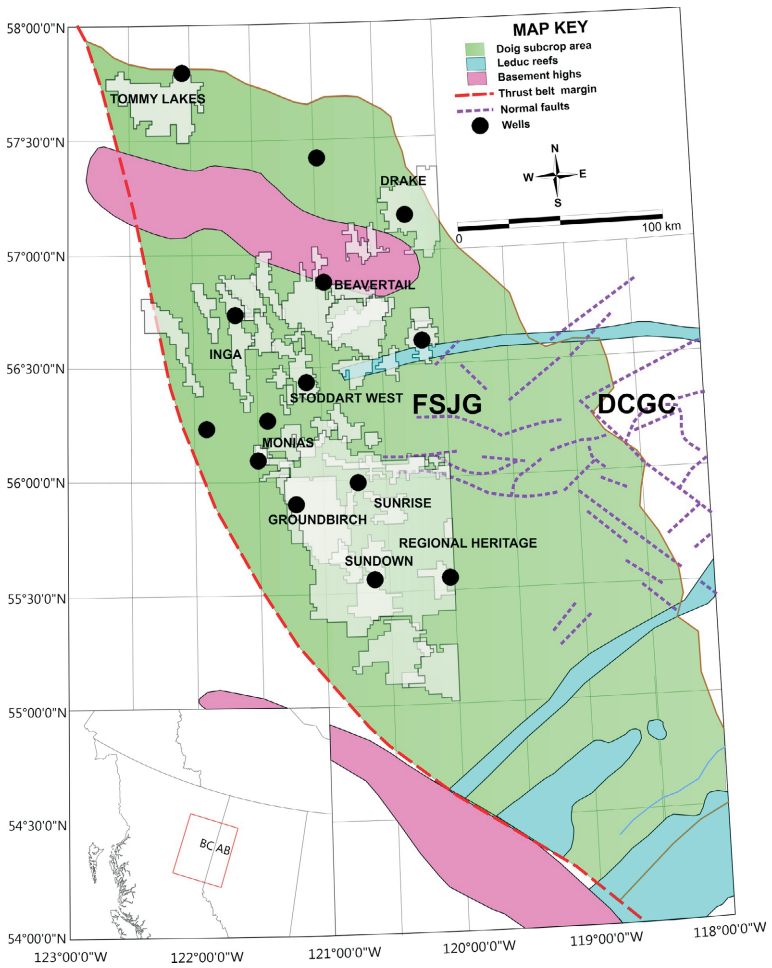

Figure 2. Location of wells from which core samples were analyzed for this study of the Doig Formation, northeastern British Columbia, against a backdrop of the Doig subcrop and main structural elements that influenced the Triassic deposition (structural elements after Davies, 1997). Abbreviations: DCGC, Dawson Creek graben complex; FSJG, Fort St. John graben.

The Doig Formation consists of mudstone, siltstone and subordinate sandstone, bioclastic packstone and grainstone, deposited under marine conditions in environments ranging from shoreface through offshore (Evoy and Moslow, 1995). The Doig Formation can be informally subdivided into three units, as proposed by Chalmers and Bustin (2012): the basal unit, Doig A, also widely referred to as the DPZ, is composed of organic-rich radioactive dark mudstone with common phosphate granules and nodules, and generally easily distinguished in well logs by its high gamma-ray signature; the intermediate Doig B, primarily composed of medium to dark grey argillaceous siltstone and mudstone intercalated with localized sandstone beds; and the upper Doig C, composed of relatively organic-lean (less than 2%) siltstone and argillaceous fine-grained sandstone.

Material and Methods

Permeability measurements were performed on a total of 60 core plugs 30 mm in diameter and between 20 and 60 mm in length. The plugs were cut from full diameter core, both parallel and perpendicular to bedding, from 14 wells located across the entire extent of the Doig subcrop area in northeastern BC (Figure 2). The samples were taken from a wide range of lithofacies stratigraphically distributed through all Doig informal subzones defined in Chalmers and Bustin (2012).

The plug samples were cleaned of soluble hydrocarbons and any residual connate brine through distillation extraction with Dean–Stark-type apparatuses, using toluene as a solvent. Each sample was cleaned for approximately one week and oven-dried at 110°C for another week. The sample mass was measured before and after solvent extraction, with an observed mass loss of 0.1 to 0.5% of the initial mass. The ends of all plugs were trimmed to minimize mud-filtrate invasion effects. Plug-end surfaces were then milled in a surface grinder to create smooth, parallel faces on both ends.

Approximately 10 g of rock from a companion sample to the plugs, was crushed to a particle size of 4.8 to 2.4 mm (4–8 mesh) for mercury intrusion porosimetry. The choice of particle size is a compromise between the more limited pore accessibility of whole plugs and the larger compressibility and closure effects on more finely crushed rock (Comisky et al., 2007; Munson, 2015). These samples were also cleaned for seven days using the Dean–Stark method of distillation extraction with toluene and then oven dried for 3 days. Approximately 30 g of 500–841 μm (20 to 35 mesh) particle-size, oven-dried crushed rock was used for helium pycnometry, and another sample measuring between 30 and 50 g was used to measure bulk density by immersion in mercury. Companion samples from the remaining whole core were also collected and powdered for mineralogy and pyrolysis.

Thin sections of select samples were studied to visualize the pore structure and resolve the relationship of texture on permeability and pore-size distribution. Thin sections were impregnated with a blue-dye epoxy to highlight porosity and a dual staining technique was used to identify carbonate minerals (Huegi, 1945; Warne, 1962; Evamy, 1963; Dickson, 1965) and feldspars (Bailey and Stevens, 1960).

Pulse-Decay Permeability

Gas permeability was obtained through a pulse-decay permeameter, using helium as the probe fluid. The solvent-extracted plugs were oven-dried at 60°C for at least three days immediately before the analysis and confined in a hydrostatic Hoek-type core-cell holder, where they were initially subjected to approximately 17 MPa (2500 psi) confining pressure and 7 MPa (1000 psi) pore pressure to reproduce the lowest possible range of in situ net confining stress (NCS). A differential pressure Δp of approximately 1 MPa (150 psi) was established between the upstream and downstream ends of the core-cell holder, and the permeability was calculated based on the Δp decay with time, according to methods outlined in Cui et al. (2009). The confining pressure was then increased, in increments of approximately 7 MPa (1000 psi), to 45 MPa (6500 psi), while keeping the pore pressure constant, and the measurement was repeated to capture the upper in situ NCS limit. At least three measurements were made at different net confining pressure values. A linear fit through the permeability as a function of NCS allowed the calculation of permeability at the in situ NCS for each sample and the estimation of permeability reduction with increasing stress. The NCS was determined for every sample, by assuming a mean total stress of 93% of the overburden, which is based on estimations of horizontal stresses for the WCSB (Bell et al., 1994), and subtracting the pore pressure from the mean. The overburden pressure was calculated as the integration with depth of the bulk density well log, filling the gaps in log coverage with a linear regression of bulk density as a function of vertical depth extrapolated to the surface. The pore pressure is a simple integration of the hydrostatic gradient with depth.

Mercury-Intrusion Porosimetry

Mercury-intrusion data was collected from the companion sample of every plug, using a Micromeritics® Autopore IV 9500 Series, to a maximum pressure of 414 MPa (60 000 psi). Mercury intrusion provides a pore-throat–size distribution curve with a lower limit of 3 nm, as well as a total porosity value. The intrusion and extrusion volumes were corrected for closure and compressibility effects. Pore-throat diameter was then calculated from the corrected data for each pressure step through the modified Young-Laplace equation proposed by Washburn (1921), assuming cylindrical pore geometry, a surface-tension value of 0.485 N/m after Adam (1941) and an advancing contact angle of 130°, established by Ellison et al. (1967) for a mercury–air–quartz system. The pore-size classification terminology used here follows the scheme defined by the International Union of Pure and Applied Chemistry, according to which micropores are defined as smaller than 2 nm, mesopores range between 2 and 50 nm and macropores are larger than 50 nm (Rouquerol et al., 1994).

Unstressed Porosity

Unstressed porosity was determined on the companion sample to the core plugs by a combination of dual chamber helium pycnometry grain volume and mercury buoyancy–mercury immersion bulk volume measurements, in accordance with the American Petroleum Institute (1998) standard. Pycnometry values were averaged over four repeated measurements for each sample. The unstressed porosity values were used as a reference to calculate stressed porosity from mercury intrusion porosimetry tests.

X-Ray–Diffraction Mineralogy

Mineralogy was obtained by X-ray diffraction using powdered samples smear mounted on glass slides, prepared according to the method outlined by Munson et al. (2016). This method was demonstrated by the authors to be a viable alternative to methods requiring much longer processing times for obtaining quantitative bulk mineralogy. However, this method does not allow to distinguish between the peaks of illite and those of muscovite. The analysis was performed using normal-focus CoKα radiation on a Bruker® D8 Focus with diffraction patterns obtained over a 2θ range of 3–70° with a step size of 0.03° and a step time of 0.8 s. Analysis of the mineral phases was quantified using the Rietveld full-pattern fitting method (Rietveld, 1967) on the Bruker® AXS TOPAS v3.0 software.

Rock-Eval Pyrolysis

Samples for whole-rock pyrolysis were analyzed using a HAWK™ instrument from Wildcat Technologies, with the standard Rock-Eval pyrolysis method after Espitalié et al. (1977). Approximately 70 mg of powdered sample was pyrolyzed at a temperature rate of 25°C per minute to a peak temperature of 650°C, followed by a temperature decrease and oxidation stage at 730°C.

Results and Discussion

The Doig Formation is very heterogeneous in terms of lithofacies, mineralogy, porosity and pore size distributions. Although it is subdivided into the basal phosphatic Doig A, the intermediate mudstone Doig B and the coarser-grained siltstone Doig C, significant variability within each zone causes the matrix permeability to vary by multiple orders of magnitude in less than 20 cm. The permeability of the Doig is controlled by a complex interplay between total porosity, pore-size distribution and clay content. The phosphatic oolitic packstone and grainstone of the Doig A and the quartz-rich siltstone of Doig C tend to have the highest porosity and more favourable balance of macro- to mesopores, which make these lithofacies the best reservoirs in terms of flow capacity.

There is a large spread in matrix permeability, spanning four orders of magnitude from 10^{-5} to 10^{-1} millidarcies (mD), for a porosity range of less than 1% to nearly 15% (Figure 3). Based on this crossplot, the rocks can be divided into two groups: rocks with porosity larger than 5% have permeabilities of 10^{-3} to 10^{-1} mD, and are essentially composed of quartz-rich siltstone to very fine sandstone (illustrated by samples TG19 and TB1) and phosphatic oolitic packstone to grainstone (illustrated by samples CD15 and MH7): the rocks of the second group have porosities ranging from just under 1 to 5% and a larger spread in permeability, ranging from 10^{-5} to 10^{-1} mD. This spread is attributed to enhanced permeability due to microfractures and degrades the correlation between porosity and permeability, which has an R^2 value of 0.27 for the linearized permeability using its logarithm. However, there is a clear trend of increasing permeability with porosity and, for all the properties measured, porosity is still the best single predictor for permeability. Pore-size distribution and, more subordinately, clay content comprise a second order control on permeability. Clay mineralogy is predominantly composed of illite, followed in importance by chlorite in the Doig C interval.

The range of permeabilities found in this study is higher than previously reported ranges of 10^{-7} to 10^{-3} mD (Chalmers and Bustin, 2012; Chalmers et al., 2012) using methane. The higher permeabilities of this study may be due to the solvent extraction process, which clears additional pathways for gas flow and/or to the smaller kinetic diameter of helium compared to methane. This study confirms the observation by Chalmers and Bustin (2012) that there is no obvious relationship between mineralogy and permeability, with the exception of clay content (Figure 4). The highest porosities and permeabilities (10^{-3} to 10^{-1} mD) are associated with the siltstone to very fine sandstone of Doig C in the Groundbirch and Beavertail areas, and the phosphatic oolitic packstone to grainstone of Doig A in the Drake and Regional Heritage fields. The relationship between permeability and mineralogy is further obscured by the occurrence of clay and extensive carbonate replacement associated with the phosphatic oolitic packstone and grainstone, which may also be associated with relatively high total organic carbon (TOC). Hence, there is no relationship between TOC and permeability. Furthermore, the quartz-rich siltstone and very fine sandstone contain a significant amount of carbonate cement. Thus, high permeabilities occur in carbonate-rich, quartz-rich and even in relatively clay-rich samples, with up to 20 wt. % clay content.

In the Groundbirch sample (TG19), porosity is mainly primary intergranular, whereas in the Beavertail sample (TB1), porosity is intergranular but mainly secondary due to dissolution of feldspar. The Groundbirch field is located at a deeper part of the basin than the Beavertail. At a burial depth of 2540 m, the porosity of sample TG19 is less than half that of sample TB1, which was retrieved from 1310 m. This helps explain the difference in permeability of one order of magnitude for these lithologically similar samples. Another factor influencing the higher permeability of TB1 is the higher proportion of macropores as opposed to mesopores (Figure 5). Both high permeability samples have over 80% of their total pore volume accessible by pore throats larger than the macropore–mesopore boundary of 50 nm. The phosphatic oolitic packstone and grainstone have pore-size distributions shifted toward the mesoporous region. However, the distributions are either broader (MH7) or weakly bimodal (CD15), which enhances permeability, likely due to the interconnectedness of macropores through mesopores. This bimodality is a result of the presence of macropores produced by partial grain dissolution of ooids and mesoporous intergranular porosity. The low permeability rocks ($<10^{-3}$ mD) have 50% or more of their total pore volume accessible through the mesoporous region or finer and are composed mostly of finer grained siltstone with highly variable proportions of clay, carbonate in the form of cement and bioclasts, and organic matter. Although mercury porosimetry is limited to pore-throat diameters larger than 3 nm, the HM1 and PA7 samples may have a significant contribution to their pore volume from micropores, as suggested by the asymptotic character of their cumulative pore-size distribution curve at the micropore–mesopore boundary.

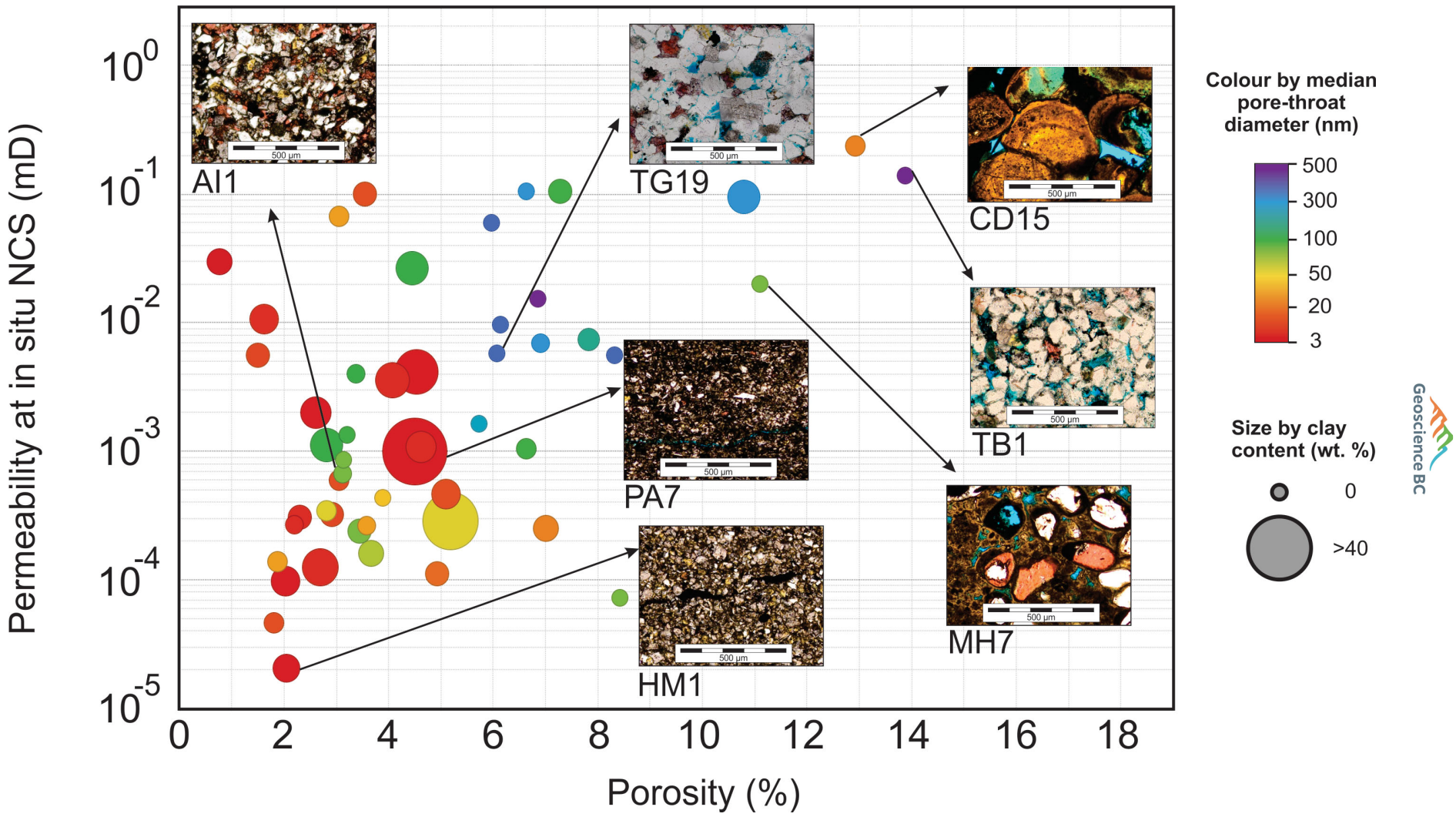

Figure 3. Crossplot of gas permeability at in situ net confining stress (NCS) versus porosity in samples analyzed for this study of the Doig Formation, northeastern British Columbia. Circle size is proportional to the total amount of clay and colour represents the median pore-throat diameter. Selected samples are highlighted to illustrate the textural variability, and its influence on porosity and permeability. Abbreviation: mD, millidarcy.

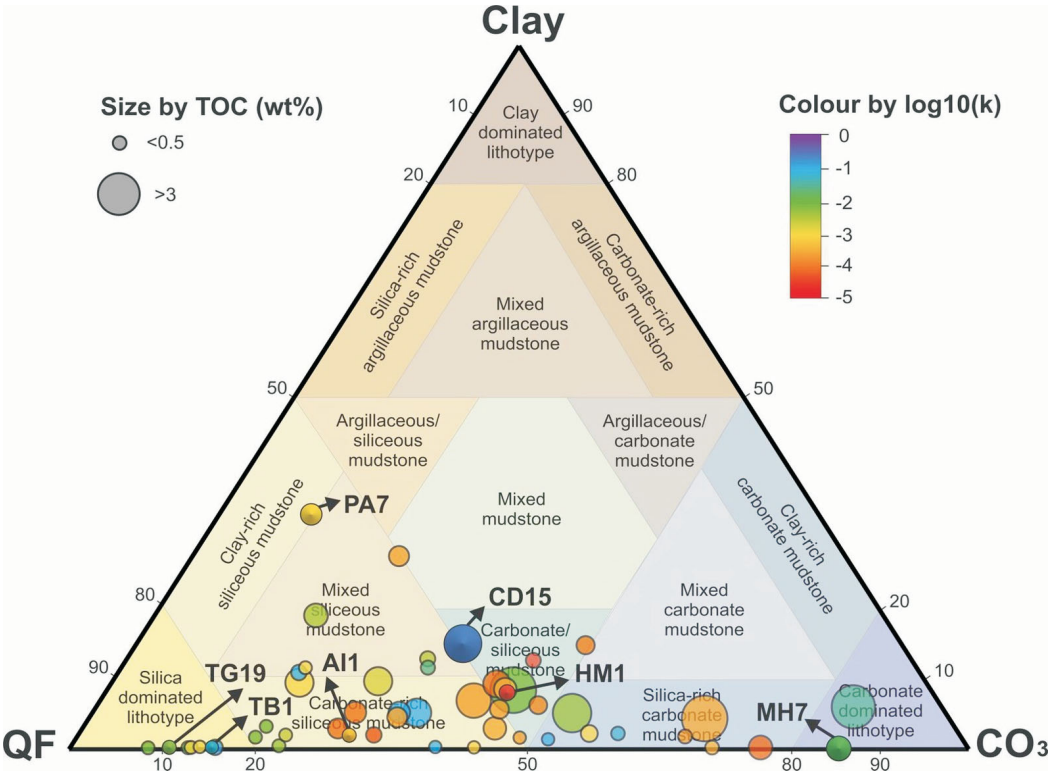

Figure 4. Ternary diagram of whole-rock mineralogy normalized to clay, carbonate and quartz-feldspar-plagioclase (QF; after Gamero-Diaz et al., 2012) of samples analyzed for this study of the Doig Formation, northeastern British Columbia. Total organic carbon (TOC) is represented by the size of the circles and the logarithm of gas permeability is represented as a colour gradient. Samples highlighted in Figures 3 and 5 are labelled.

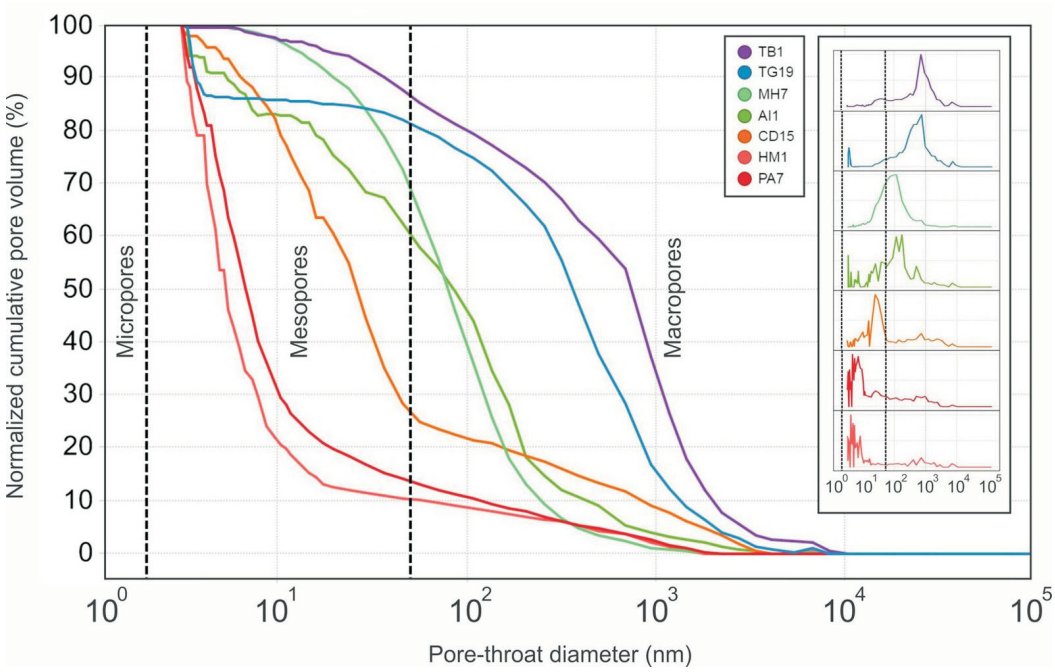

Figure 5. Curves of cumulative pore-throat diameter normalized to total pore volume of the selected samples highlighted in Figure 3 for this study of the Doig Formation, northeastern British Columbia. Inset shows their respective frequency distributions sorted by pore size, in descending order from the top.

Ongoing Work

This study is part of a larger research project aimed at characterizing the Doig Formation through a petroleum system analysis approach and evaluating its potential (Silva, 2017). The project includes an assessment of the source-rock organic geochemical properties, storage and flow properties, geomechanical behaviour, and basin modelling focused on the reconstruction of the thermal history and timing of hydrocarbon generation. Besides the other components of the project, the next steps in characterizing the permeability are:

- inspecting for fractures under the microscope and through acetone imbibition, on the anomalously high permeabilities exhibited by dominantly clay-rich mesoporous samples that plot off trend;
- understanding the impact of the solvent-extraction process on the gas-permeability measurements, which may help explain the discrepancy between the range of permeabilities found in this study and the ones from previous studies, besides providing important information on sample-preparation procedures for mudrock, which currently lack consensus and data;
- characterizing the microporous portion of pore-size distributions of lower permeability (10^{-5} to 10^{-3} mD) samples, which is below the resolution of mercury porosimetry, through low-pressure isotherms; and
- carrying out additional matrix-permeability measurements on samples from different lithofacies, which will assist in better understanding the impact on permeability of the interplay between porosity, pore-size distribution, mineralogy and lithology, and which may help in defining distinct porosity–permeability functions for difference lithofacies.

Acknowledgments

The authors acknowledge financial support from Geoscience BC, Canadian Natural Resources Limited, Chevron Canada Limited, Devon Energy Corporation, EnCana Corporation, geoLOGIC systems ltd., Husky Energy Inc. and AGAT Laboratories. The donation of software by geoLOGIC systems ltd. and Paradigm Geophysical Canada Limited was also instrumental in handling the well and core data, and greatly appreciated. The authors would also like to acknowledge the time and effort dedicated to the thorough review of the manuscript by G. Chalmers, research associate at The University of British Columbia.

References

Adam, N.K. (1941): The Physics and Chemistry of Surfaces (3rd edition); Oxford University Press, Oxford, 448 p.

American Petroleum Institute (1998): Recommended Practice RB40: Recommended Practices for Core Analysis; API Publishing Services, Washington, DC, 236 p., URL <http://w3.energistics.org/RP40/rp40.pdf> [October 2018].

Armitage, J.H. (1962): Triassic oil and gas occurrences in northeastern British Columbia, Canada; Journal of the Alberta Society of Petroleum Geologists, v. 10, p. 35–56.

Bailey, E.H. and Stevens, R.E. (1960): Selective staining of K-feldspar and plagioclase on rock slabs and thin sections; The American Mineralogist, v. 45, p. 1020–1025.

Barclay, J.E., Krause, F.F., Campbell, R.I. and Utting, J. (1990): Dynamic casting of the Dawson Creek Graben Complex: Carboniferous-Permian Peace River Embayment, western Canada; Bulletin of Canadian Petroleum Geology, v. 38(A), p. 115–145.

Bell, J.S., Price, P.R. and McLellan, P.J. (1994): In-situ stress in the Western Canada Sedimentary Basin; *in* Geological Atlas of the Western Canada Sedimentary Basin, G.D. Mossop and I. Shetsen (comp.), Canadian Society of Petroleum Geologists and Alberta Research Council, Edmonton, Alberta, p. 439–446, URL <https://www.cspg.org/documents/Publications/Atlas/geological/atlas_29_in-situ_stress_in_the_WCSB.pdf> [October 2018].

Chalmers, G.R.L. and Bustin, R.M. (2012): Geological evaluation of Halfway-Doig-Montney hybrid gas shale-tight gas reservoir, northeastern British Columbia; Marine and Petroleum Geology, v. 38, no. 1, p. 53–72.

Chalmers, G.R.L., Bustin, R.M. and Bustin, A.A.M. (2012): Geological controls on matrix permeability of the Doig–Montney hybrid shale-gas–tight-gas reservoir, northeastern British Columbia (NTS 093P); *in* Geoscience BC Summary of Activities 2011, Geoscience BC Report 2012-1, p. 87–96, URL <https://cdn.geoscience bc.com/pdf/SummaryofActivities2011/SoA2011_Chalmers.pdf> [October 2018].

Chopra, S., Kumar Sharma, R. and Keay, J. (2014): Mapping Middle Triassic Doig sandstone reservoirs in northeast British Columbia using seismic attributes; Society of Exploration Geophysicists, 2013 SEG Annual Meeting, September 22–27, 2013, Houston, Texas, SEG-2013-0170, URL <https://www.onepetro.org/conference-paper/SEG-2013-0170> [October 2018].

Comisky, J.T., Newsham, K.E., Rushing, J.A. and Blasingame, T.A. (2007): A comparative study of capillary-pressure-based empirical models for estimating absolute permeability in tight gas sands; Society of Petroleum Engineers, 2007 SPE Annual Technical Conference and Exhibition, November 11–14, 2007, Anaheim, California, SPE-110050-MS, URL <https://www.onepetro.org/conference-paper/SPE-110050-MS> [October 2018].

Creaney, S. and Allan, J. (1990): Hydrocarbon generation and migration in the Western Canada Sedimentary Basin; *in* Classic Petroleum Provinces, J. Brooks (ed.), Geological Society of London, Geological Society Special Publications 50, p. 189–202.

Cui, X., Bustin, A.M.M. and Bustin, R.M. (2009): Measurements of gas permeability and diffusivity of tight reservoir rocks: different approaches and their applications; Geofluids, v. 9, p. 208–223.

Davies, G.R. (1997): The Triassic of the Western Canada Sedimentary Basin: tectonic and stratigraphic framework, paleogeography, paleoclimate and biota; Bulletin of Canadian Petroleum Geology, v. 45, no. 4, p. 434–460.

Dickson, J.A.D. (1965): A modified staining technique for carbonates in thin section; Nature, v. 205, p. 587.

Du Rouchet, J. (1985): The origin and migration paths of hydrocarbons accumulated in the Lower Cretaceous sandstone 'giant' tar accumulations of Alberta–Part II; Journal of Petroleum Geology, v. 8, no. 1, p. 101–114.

Eaton, D.W., Ross, G.M. and Hope, J. (1999): The rise and fall of a cratonic arch: a regional seismic perspective on the Peace River Arch, Alberta; Bulletin of Canadian Petroleum Geology, v. 47, no. 4, p. 346–361.

Edwards, D.E., Barclay, J.E., Gibson, D.W., Kvill, G.E. and Halton, E. (1994): Triassic strata of the Western Canada Sedimentary Basin; Chapter 16 *in* Geological Atlas of the Western Canada Sedimentary Basin, G.D. Mossop and I. Shetsen (comp.), Canadian Society of Petroleum Geologists and Alberta Research Council, Edmonton, Alberta, p. 257–275, URL <https://ags.aer.ca/publications/chapter-16-triassic-strata> [October 2018].

Ellison, A.H., Klemm, R.B., Schwartz, A.M., Grubb, L.S. and Petrash, D.A. (1967): Contact angles of mercury on various surfaces and the effect of temperature; Journal of Chemical and Engineering Data, v. 12, no. 4, p. 607–609.

Espitalié, J., Laporte, J.L., Madec, M., Marquis, F., Leplat, P., Paulet, J. and Boutefeu, A. (1977): Méthode rapide de caractérisation des roches mères, de leur potentiel pétrolier et de leur degré d'évolution; Revue de l'Institut Français du Pétrole, v. 32, no. 1, p. 23–42.

Evamy, B.D. (1963): The application of a chemical staining technique to a study of dedolomitisation; Sedimentology, v. 2, p. 164–170.

Evoy, R.W. and Moslow, T.F. (1995): Lithofacies associations and depositional environments in the Middle Triassic Doig Formation, Buick Creek Field, northeastern British Columbia; Bulletin of Canadian Petroleum Geology, v. 43, no. 4, p. 461–475.

Faraj, B., Harold, W., Addison, G., McKinstry, B., Donaleshen, R., Sloan, G., Lee, J., Anderson, T., Leal, R., Anderson, C., Lafleur, C. and Ahlstrom, A. (2002): Shale gas potential of selected Upper Cretaceous, Jurassic, Triassic and Devonian shale formations in the WCSB of Western Canada: implications for shale gas production; Gas Technology Institute, Report GRI-02/0233, 258 p.

Gamero-Diaz, H., Miller, C. and Lewis, R. (2012): sCore: A classification scheme for organic mudstones based on bulk mineralogy; American Association of Petroleum Geologists, AAPG Southwest Section Convention, May 19–22, 2012, Fort Worth, Texas, AAPG Search and Discovery article 40951, 18 p., URL <https://www.searchanddiscovery.com/documents/2012/40951diaz/ndx_diaz.pdf> [October 2018].

Gibson, D.W. and Barclay, J.E. (1989): Middle Absaroka sequence–the Triassic stable craton; *in* Western Canada Sedimentary Basin–a Case History, B.D. Ricketts (ed.), Canadian Society of Petroleum Geologists, Calgary, Special Publication, p. 219–232.

Golding, M.L., Orchard, M.J., Zonneveld, J.P. and Wilson, N.S.F. (2015): Determining the age and depositional model of the Doig phosphate zone in northeastern British Columbia using conodont biostratigraphy; Bulletin of Canadian Petroleum Geology, v. 63, no. 2, p. 143–170.

Hardenbol, J., Thierry, J., Farley, M.B., Jacquin, T., De Graciansky, P.-C. and Vail, P.R. (1998): Cenozoic sequence chronostratigraphy; *in* Mesozoic and Cenozoic Sequence Chronostratigraphic Framework of European Basins, P.C. De Graciansky, J. Hardenbol, T. Jacqui and P.R. Vail (ed.), Society for Sedimentary Geology, SEPM Special Publication 60, p. 3–13.

Henderson, C.M. (1989): The lower Absaroka Sequence: Upper Carboniferous and Permian; *in* Western Canada Sedimentary Basin–a Case History, Special Publication, B.D. Ricketts (ed.), Canadian Society of Petroleum Geologists, Calgary, p. 203–217.

Huegi, T. (1945): Gesteinbildend wichtige karbonate und deren nachweis mittels farbmethoden; Schweizerische Mineralog und Petrographische Mitteilungen, v. 25, p. 114–140.

Marshall, G.M., Noble, I.A.R. and Tang, C.W. (1987): Triassic/Jurassic fields; Chapter 7 *in* Geophysical Atlas of Western Canadian Hydrocarbon Pools, N.L. Anderson, L.V. Hills and D.A. Cederwall (ed.), Canadian Society of Exploration Geophysicists and Canadian Society of Petroleum Geologists, Calgary, Alberta, p. 187–215, URL <https://www.cspg.org/cspg/documents/Publications/Atlas/geophysical/L_Chapter_7.pdf> [October 2018].

Munson, E.O. (2015): Reservoir characterization of the Duvernay Formation, Alberta: a pore- to basin-scale investigation; Ph.D. thesis, University of British Columbia, 266 p.

Munson, E.O., Chalmers, G.R.L., Bustin, R.M. and Li, K. (2016): Utilizing smear mounts for X-ray diffraction as a fully quantitative approach in rapidly characterizing the mineralogy of shale gas reservoirs; Journal of Unconventional Oil and Gas Resources, v. 14, p. 22–31.

Riediger, C.L., Fowler, M.G., Brooks, P.W. and Snowdon, L.R. (1990): Triassic oils and potential Mesozoic source rocks, Peace River Arch area, Western Canada Basin; Organic Geochemistry, v. 16, no. 1–3, p. 295–305.

Rietveld, H.M. (1967): Line profiles of neutron powder-diffraction peaks for structure refinement; Acta Crystallographica, v. 22, p. 151–152.

Rouquerol, J., Avni, D., Fairbridge, C.W., Everett, D.H., Haynes, J.M., Pernicone, N., Ramsay, J.D.F., Sing, K.S.W. and Unger, K.K. (1994): Recommendations for the characterization of porous solids; International Union of Pure and Applied Chemistry, v. 68, no. 8, p. 1739–1758.

Silva, P.L. (2017): Status report on petroleum system analysis study of the Triassic Doig Formation, Western Canada Sedimentary Basin, northeastern British Columbia; *in* Geoscience BC Summary of Activities 2011, Geoscience BC Report 2017-1, p. 25–28, URL <https://cdn.geosciencebc.com/pdf/SummaryofActivities2016/SoA2016_Silva.pdf> [October 2018].

United States Energy Information Administration (2013): Technically recoverable shale oil and shale gas resources: Canada; United States Department of Energy, 29 p., URL <https://www.eia.gov/analysis/studies/worldshalegas/pdf/overview.pdf> [October 2018].

Walsh, W., Adams, C., Kerr, B. and Korol, J. (2006): Regional "shale gas" potential of the Triassic Doig and Montney formations, northeastern British Columbia; BC Ministry of Energy, Mines and Petroleum Resources, Oil and Gas Division, Resource Development and Geoscience Branch, Open File 2006-0, 19 p., URL <https://www2.gov.bc.ca/assets/gov/farming-natural-resources-and-industry/natural-gas-oil/petroleum-geoscience/petroleum-open-files/pgof20062.pdf> [October 2018].

Warne, S.S.J. (1962): A quick field or laboratory staining scheme for the differentiation of the major carbonate minerals; Journal of Sedimentary Petrology, v. 32, p. 29–38.

Washburn, E.W. (1921): Note on a method of determining the distribution of pore sizes in a porous material; *in* Proceedings of the National Academy of Sciences of the United States of America, v. 7, no. 4, p. 115–116.